



HAL
open science

Analysis of the whispering gallery mode sapphire Fe³⁺ maser under magnetic field

M. Mrad, P.-Y. Bourgeois, M. E. Tobar, Y. Kersalé, V. Giordano

► **To cite this version:**

M. Mrad, P.-Y. Bourgeois, M. E. Tobar, Y. Kersalé, V. Giordano. Analysis of the whispering gallery mode sapphire Fe³⁺ maser under magnetic field. *European Physical Journal: Applied Physics*, 2012, 57 (2), pp.21005. 10.1051/epjap/2012110366 . hal-00686948

HAL Id: hal-00686948

<https://hal.science/hal-00686948>

Submitted on 5 May 2021

HAL is a multi-disciplinary open access archive for the deposit and dissemination of scientific research documents, whether they are published or not. The documents may come from teaching and research institutions in France or abroad, or from public or private research centers.

L'archive ouverte pluridisciplinaire **HAL**, est destinée au dépôt et à la diffusion de documents scientifiques de niveau recherche, publiés ou non, émanant des établissements d'enseignement et de recherche français ou étrangers, des laboratoires publics ou privés.



Distributed under a Creative Commons Attribution 4.0 International License

Analysis of the whispering gallery mode sapphire Fe^{3+} maser under magnetic field

M. Mrad¹, P.Y. Bourgeois¹, M.E. Tobar², Y. Kersalé^{1,a}, and V. Giordano¹

¹ FEMTO-ST Institute, Time and Frequency Department, UMR 6174 CNRS, ENSMM, 26 Chemin de l'Épitaphe, 25030 Besançon Cedex, France

² University of Western Australia, School of Physics, Crawley 6009, WA, Australia

Abstract. This article describes the influence of the magnetic field on a small amount of residual Fe^{3+} ion impurities contained in a sapphire resonator excited on a whispering gallery mode and cooled down to 4 K. The energy levels and transition probabilities between pairs of levels of the system are calculated in order to determine the effect of the magnetic field on the maser output power and also on the pump power threshold.

1 Introduction

The need for microwave sources exhibiting ultra-high spectral purity and high temporal stability is a key point highlighted by the performance limitations in major strategic applications such as radar, spatial communications, ultra-high accuracy navigation system and high bitrate optical telecommunications. The Cryogenic Sapphire Oscillator (CSO) is currently the only microwave technology able to provide a relative frequency stability better than 1×10^{-14} for integration time between 1 s and 10^4 s [1, 2]. Nevertheless, the CSO remains a complex instrument and needs several servo loops to control the oscillator phase and the microwave power incident on the resonator. Recently, we reported in [3, 4] the possibility to use the sapphire resonator in another way. Here, the sustaining amplification is achieved through the interaction between a whispering gallery mode and the paramagnetic Fe^{3+} ions also present in the sapphire crystal. The frequency instability of the Whispering Gallery Mode maser is limited to 10^{-14} due to the measurement readout [5].

In the sapphire crystal, the Fe^{3+} ion exhibits three energy states at zero magnetic field enabling to realize a self-sustaining solid-state maser. For a maser the ultimate limit in terms of frequency instability is the Schawlow-Townes limit [6] which is inversely proportional to the square root of the maser output power. As a consequence to decrease the frequency instability we have to increase the maser output power.

In this paper we describe, theoretically, the effect of a magnetic field on the Whispering Gallery Mode (WGM) maser oscillator and we show that in a particular

configuration the maser output power can be increased by a factor of 6 dB.

2 Principle

Maser materials, and maser operations were introduced in the 1950s by several groups [7–10]. In particular, the action of iron ions in corundum was studied by Friedman and Nagy [11]. The corundum used for this experiment was of poor quality, and as a consequence the iron doping was deliberately strong. Recently we have demonstrated that high-quality sapphire resonator with a small amount of paramagnetic impurities (Fe^{3+} ions) can provide a maser signal with an output power of -30 dBm [12]. The maser fundamental limit is defined by [6, 13]:

$$\sigma_y(\tau) = \frac{1}{Q_{signal}} \sqrt{\frac{k_B T}{2P_{out}\tau}} \quad (1)$$

with Q_{signal} being the loaded Q -factor of the considered mode, P_{out} the power in watts at the maser output, k_B the Boltzmann constant and T the temperature of the amplifying medium. As we can see in equation (1) to get the best frequency instability we have to maximize the maser output power. In order to maximize it we have studied the effect of the magnetic field (orientation and amplitude) on the pump power threshold and on the maser output power.

2.1 Fe^{3+} Characteristics

The Fe^{3+} ion has the $[\text{Ar}]3d^5$ electronic configuration. The number of total spins is $S = 5/2$, the total orbital number

^a e-mail: yann.kersale@femto-st.fr

is $L = 0$ and the spectroscopic ground state term is 6S . The Fe^{3+} ion replaces the cation Al^{3+} in the crystal and undergoes the action of a crystal field of the nearby ions O^{2-} and Al^{3+} .

These interactions are described by the following Hamiltonian:

$$\begin{aligned} \hat{H} = & g\mu_B H \hat{S} + D \left[\hat{S}_Z^2 - \frac{1}{3} S(S+1) \right] \\ & + \frac{1}{6} a \left[\hat{S}_\xi^4 + \hat{S}_\eta^4 + \hat{S}_\zeta^4 - \frac{1}{5} S(S+1)(3S^2 + 3S - 1) \right] \\ & + \frac{1}{180} F \left[35\hat{S}_Z^4 - 30S(S+1)\hat{S}_Z^2 \right. \\ & \left. + 25\hat{S}_Z^2 - 6S(S+1) + 3S^2(S+1) \right]. \end{aligned} \quad (2)$$

To calculate this Hamiltonian we have considered the crystal cubic field with trigonal distortion and the axis (Z) as axis of symmetry, which is the case of our resonators. Indeed, corundum $\alpha\text{-Al}_2\text{O}_3$ crystallizes in the rhombohedral system. (ξ, η, ζ) are the axes of the trigonal crystal field. The crystalline axis of symmetry (C_3) = (Z) is defined in the direction (1, 1, 1) of this system. For more details on the structure of corundum, see [8,9].

The energy levels are calculated based on the parameters “ D ”, “ F ” and “ a ” in the above equation. “ D ” and “ F ” are the parameters of the axial field, respectively, second and fourth order, and the spacing between levels is primarily due to “ D ”. “ a ” is the parameter of trigonal field (mixing between the levels E_1 and E_3 of the system). The values of these parameters, measured at 4 K by Symmons and Bogle [14], are equal to: $D = 1719.2 \pm 1$, $|a| = 229.4 \pm 1$ and $a - F = 341.5 \pm 1$ expressed in 10^{-4} cm^{-1} . We assumed that $h_i = g_j \times \mu_B \times H_i$, where the indices are respectively $i = x, y$ and Z and $j = \perp, \perp$ and \parallel , g is the Lande factor and μ_B the Bohr magneton. We will also consider that $h^\pm = h_x \pm ih_y = g_\perp \times \mu_B (H_x \pm iH_y)$, $\gamma = a - F$ and $p = (2\sqrt{5}/3)a$. Moreover for our system ($S = 5/2$) the factor $\frac{1}{3}S(S+1) = 35/12$.

The matrix Hamiltonian of the Fe^{3+} ion in sapphire can now be written as follows: see equation (3) in the next page.

2.2 Energy levels

The matrix in equation (3) was numerically solved in order to determine the eigenstates and eigenvalues of this system. In order to verify if our numerical model is correct we plot (Fig. 1) the evolution of the energy levels as a function of a magnetic field applied in the parallel direction of the crystal axis.

The energy levels of the Fe^{3+} ions in the sapphire lattice represented here are very similar to what has been published before [15] and so we can consider that our numerical model is correct.

In the next plot we have represented the energy levels for a magnetic field perpendicular to the crystal axis (see Fig. 2).

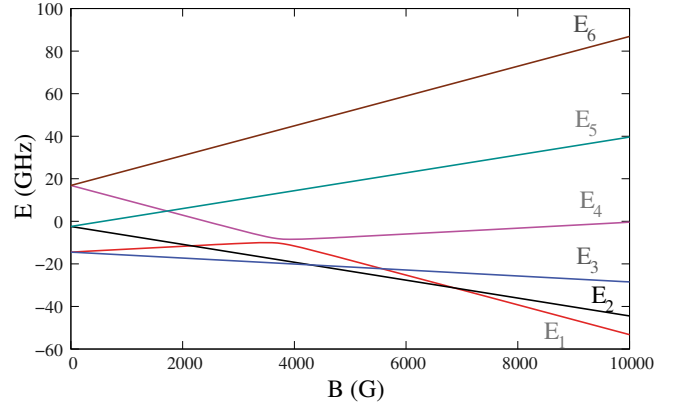


Fig. 1. (Color online) Energy level variations of the Fe^{3+} ion in alumina as a function of a magnetic field parallel to the crystal Z -axis.

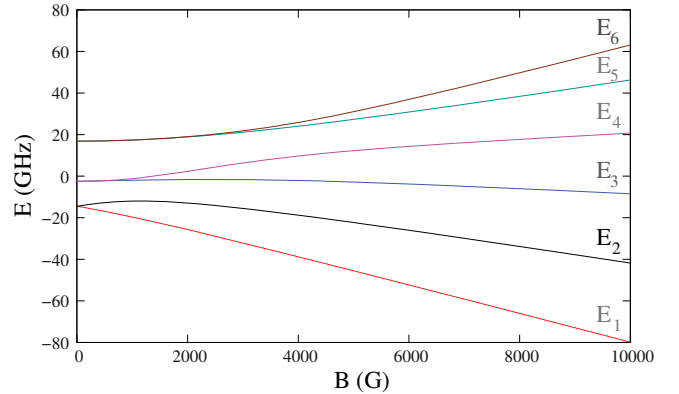


Fig. 2. (Color online) Energy levels variations of the Fe^{3+} ion in alumina as a function of a magnetic field perpendicular to the crystal Z -axis.

When the magnetic field is parallel to the Z -axis all the levels are immediately split when the value of the field increases. As opposed, when the field is perpendicular to the crystal axis, and with a value of 50 G, states 5 and 6 are separated by 450 kHz as well as levels 3 and 4 while states 1 and 2 are separated by more than 400 MHz. Considering the Electronic Spin Resonance (ESR) bandwidth of 100 MHz [12] we can consider that the two upper states (i.e., levels 5 and 6) are mixed and the two lower states can be considered completely separated and so on, ions pumped from the level 1 to levels 5 and 6 will participate in the maser action.

A zoom on the prevision plot leads us to determine the transition frequencies of the system under magnetic field (see Fig. 3).

The transition frequencies of the system with a magnetic field of 50 G oriented in the perpendicular plane of the crystal are a little bit different from the values with zero magnetic field. We get: $\nu_{14} = 12.2676 \text{ GHz}$ (12.037 GHz with no magnetic field) and $\nu_{16} = 31.5647 \text{ GHz}$ (31.318 GHz with no magnetic field). We will now assume that our sapphire resonator have whispering gallery modes centered on the ν_{14} transition and another one centered between ν_{15} and ν_{16} at 31.5645 GHz.

$$\hat{H} = \begin{pmatrix} -\frac{5}{2}h_Z - \frac{1}{3}\gamma + \frac{10}{3}D & \frac{\sqrt{5}}{2}h^+ & 0 & \pm ip & 0 & 0 \\ \frac{\sqrt{5}}{2}h^- & -\frac{3}{2}h_Z + \gamma - \frac{2}{3}D & \sqrt{2}h^+ & 0 & 0 & 0 \\ 0 & \sqrt{2}h^- & -\frac{1}{2}h_Z - \frac{2}{3}\gamma - \frac{8}{3}D & \frac{3}{2}h^+ & 0 & \mp ip \\ \mp ip & 0 & \frac{3}{2}h^- & \frac{1}{2}h_Z - \frac{2}{3}\gamma - \frac{8}{3}D & \sqrt{2}h^+ & 0 \\ 0 & 0 & 0 & \sqrt{2}h^- & \frac{3}{2}h_Z + \gamma - \frac{2}{3}D & \frac{\sqrt{5}}{2}h^+ \\ 0 & 0 & \pm ip & 0 & \frac{\sqrt{5}}{2}h^- & \frac{5}{2}h_Z - \frac{1}{3}\gamma + \frac{10}{3}D \end{pmatrix} \quad (3)$$

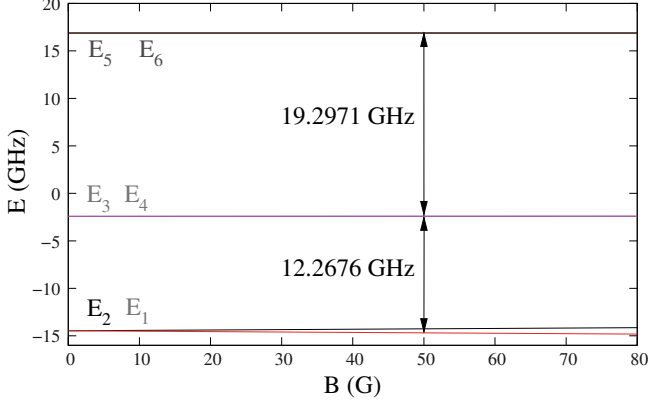


Fig. 3. (Color online) Zoom on the energy levels variations of the Fe^{3+} ion in alumina as a function of a magnetic field perpendicular to the crystal Z -axis.

These can be realized by machining the radius of our actual resonator centered at 12.037 GHz and 31.318 GHz. Under this configuration we consider now that the maser output signal will operate between levels 4 and 1 and the pump signal will be applied between the level 1 and the mixed states 5 and 6.

3 General populations of the system under field

3.1 Population differences at thermal equilibrium

When there is no magnetic field applied, the Fe^{3+} ion gets three energy levels in the sapphire lattice and with an applied magnetic field each state splits in two states with respect to the Zeeman effect. At thermal equilibrium the level populations have the Boltzmann relationships [10]:

$$\frac{N_j}{N_i} = \exp\left(-\frac{h\nu_{ij}}{k_B T}\right) = e^{-\Delta_{ij}} \quad \text{and} \quad \sum_{i=1}^6 N_i = N, \quad (4)$$

where N is the total number of spins and $\Delta_{ij} = -\Delta_{ji}$ with $i, j = 1, 2, 3, 4, 5$ and 6.

The population differences at the thermal equilibrium can thus be expressed as:

$$\Delta N_{ij} = N_i - N_j = \frac{1 - e^{-\Delta_{ij}}}{\sum_{k=1}^6 e^{-\Delta_{ik}}} \times N. \quad (5)$$

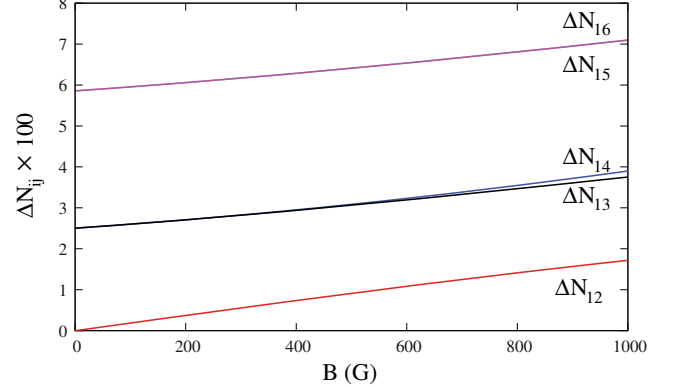


Fig. 4. (Color online) Population differences of the Fe^{3+} ion in alumina as a function of a magnetic field perpendicular to the crystal Z -axis.

Figure 4 represents the population differences at 4.2 K as a function of the magnetic field perpendicular to the crystal axis.

From this plot we get: $\Delta N_{12} = 0.09332 \times 10^{-2} \times N$; $\Delta N_{13} = 2.55064 \times 10^{-2} \times N$; $\Delta N_{14} = 2.55066 \times 10^{-2} \times N$; $\Delta N_{15} = 5.90472 \times 10^{-2} \times N$; $\Delta N_{16} = 5.90479 \times 10^{-2} \times N$.

3.2 Rate equation for a six-level system

The rate equations of this system are expressed as follows:

$$\begin{aligned} \frac{dn_1}{dt} &= - \sum_{j \neq 1}^6 \frac{\Delta n_{1j} - \Delta N_{1j}}{2\tau_1^{(1j)}} - W_S \Delta n_{14} - W_{15} \Delta n_{15} \\ &\quad - W_{16} \Delta n_{16}, \\ \frac{dn_2}{dt} &= - \sum_{j \neq 2}^6 \frac{\Delta n_{2j} - \Delta N_{2j}}{2\tau_1^{(2j)}} - W_{25} \Delta n_{25} - W_{26} \Delta n_{26}, \\ \frac{dn_3}{dt} &= - \sum_{j \neq 3}^6 \frac{\Delta n_{3j} - \Delta N_{3j}}{2\tau_1^{(3j)}}, \\ \frac{dn_4}{dt} &= - \sum_{j \neq 4}^6 \frac{\Delta n_{4j} - \Delta N_{4j}}{2\tau_1^{(4j)}} + W_S \Delta n_{14}, \\ \frac{dn_5}{dt} &= - \sum_{j \neq 5}^6 \frac{\Delta n_{5j} - \Delta N_{5j}}{2\tau_1^{(5j)}} + W_{15} \Delta n_{15} + W_{25} \Delta n_{25}, \\ \frac{dn_6}{dt} &= - \sum_{j \neq 6}^6 \frac{\Delta n_{6j} - \Delta N_{6j}}{2\tau_1^{(6j)}} + W_{16} \Delta n_{16} + W_{26} \Delta n_{26}, \end{aligned} \quad (6)$$

where W_{ij} represents the rate absorption, and τ_1^{ij} the spin lattice relaxation time of the Fe^{3+} ion in the sapphire lattice between levels i and j . We will then assume that $\tau_1^{ij} = \tau_1 \forall i, j$ and is equal to 10 ms [8, 16, 17] at the liquid helium temperature.

To determine the steady state of this system ($dn_i/dt = 0$) we have to consider equation (7) which is the sum of population differences:

$$\Delta n_{12} + \Delta n_{23} + \Delta n_{34} + \Delta n_{45} + \Delta n_{56} - \Delta n_{16} = 0. \quad (7)$$

The maser output frequency and the stimulated emission rate (i.e., between levels 1 and 4) will be denoted by ν_S and W_S and for the pump signal (i.e., from level 1 to levels 5 and 6) will be denoted by ν_p and W_p with:

$$\nu_p = \frac{\nu_{15} + \nu_{16}}{2}; \quad W_p = \frac{W_{15} + W_{16}}{2}. \quad (8)$$

Finally, the stationary solutions of the system are:

$$\Delta n_{14} = \frac{-3(\Delta N_{15} + \Delta N_{16})\tau_1 W_p + 9\Delta N_{14}(1 + \tau_1 W_p)}{3(3 + (3W_p + 2W_S)\tau_1) + 4\tau_1^2 W_p W_S}, \quad (9)$$

$$\frac{\Delta n_{15} + \Delta n_{16}}{2} = \frac{9(\Delta N_{15} + \Delta N_{16}) + 6(\Delta N_{15} + \Delta N_{16} - \Delta N_{14})\tau_1 W_S}{6(3 + (3W_p + 2W_S)\tau_1) + 8\tau_1^2 W_p W_S}. \quad (10)$$

4 The maser pump and output power

In this section we will define the relation between the pump power (P_p) and the maser output power (P_{41}).

4.1 Evolution of the emitted power as a function of pump power

The maximum of power that can be emitted by a maser system is defined as [10]

$$P_{41} = h\nu_S W_S \Delta n_{41} V_{41}, \quad (11)$$

where V_{41} is the effective volume of the whispering gallery mode involved in the emission process [18].

The stimulated absorption is represented as follows [10]:

$$W_S = Q_{0s} \frac{1}{4} \gamma^2 g(\nu_{14}) H_{acsignal}^2 \sigma_{14}^2. \quad (12)$$

From the definition of the Poynting vector, the power in the resonator is directly proportional to the magnetic field. It leads to:

$$H_{acsignal}^2 = \frac{2P_{41}}{Z_c S_{eff14}}. \quad (13)$$

Therefore:

$$W_S = Q_{0s} \frac{\gamma^2 g(\nu_{14}) \sigma_{14}^2}{2Z_c S_{eff14}} P_{41} = Q_{0s} w_{S_0} P_{41}. \quad (14)$$

This representation can also be applied to the probability of absorption:

$$W_p = Q_{0p} \frac{\gamma^2 Q_{0p} g(\nu_p) \sigma_p^2}{2Z_c S_{effp}} P_p = Q_{0p} w_{p_0} P_p. \quad (15)$$

From equation (7) we can write:

$$w_{p_0} = \frac{w_{15_0} + w_{16_0}}{2} = \frac{1}{2} \frac{\gamma^2 Q_{0p} g(\nu_p) (\sigma_{15}^2 + \sigma_{16}^2)}{2Z_c S_{effp}}, \quad (16)$$

where γ is the gyromagnetic factor. S_{eff14} and S_{effp} are respectively the effective surfaces of the whispering gallery mode in the meridian resonator plane for the maser signal and the maser pump, Z_c is the characteristic resonator impedance (112 Ω), and Q_{0s} and Q_{0p} are the quality factors of the whispering gallery modes for the maser signal and the maser pump respectively [18].

From equation (9) we can now determine the maser output power (P_{41}) as a function of the pump power (P_p), with $C = h\nu_{14} w_{S_0} \Delta N_{41} V_{14}$: see equation (17) in the next page.

4.2 Pump power threshold

The pump power threshold $P_{p_{th}}$ appears when the population inversion occurs ($\Delta n_{14} = 0$). The rate absorption threshold ($W_{p_{Th}}$) is the solution of the following equation (from Eq. (8)):

$$3\tau_1 W_{p_{Th}} (3\Delta N_{14} - (\Delta N_{15} + \Delta N_{16})) + 9\Delta N_{14} = 0. \quad (18)$$

Finally we get:

$$W_{p_{Th}} = \frac{3}{\tau_1} \frac{\Delta N_{14}}{-3\Delta N_{14} + \Delta N_{15} + \Delta N_{16}} = w_{p_0} P_{p_{Th}}. \quad (19)$$

4.3 Determination of the transition probabilities and the line shape function

In order to determine the transition probabilities (W_S and W_p) of the maser and pump transitions, we have to solve the previous Hamiltonian in order to calculate σ_{ij}^2 which characterizes the strength of the transition probabilities. On the next plots we have represented the evolution of all the transition probabilities for a magnetic field perpendicular to the crystal axis (see Figs. 5–8).

In reality, if the signal is not exactly at the transition frequency, the transition probability decreases as determined by the line shape function $g(\nu)$. The line shape function is usually described by a Lorentzian or a Gaussian profile. It is a function normalized and centered around the transition frequency:

$$\int_0^\infty g(\nu) d\nu = 1. \quad (20)$$

In our case, we have proved that the Fe^{3+} ions are inhomogeneously broadened [12] and so $g(\nu)$ is represented by

$$P_{41} = \frac{3(-3(1 + P_p \tau_1 Q_{0p} w_{p0}) + C((\Delta N_{15} + \Delta N_{16})P_p \tau_1 Q_{0p} w_{p0} - 3\Delta N_{14}(1 + P_p \tau_1 Q_{0p} w_{p0})))}{2\tau_1(3 + 2P_p \tau_1 Q_{0p} w_{p0})Q_{0s} w_{S0}} \quad (17)$$

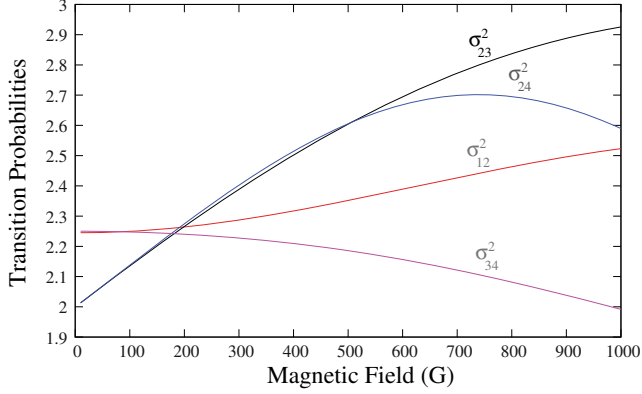


Fig. 5. (Color online) Transition probabilities (σ_{ij}^2) between levels i and j as a function of a magnetic field perpendicular to the crystal Z -axis.

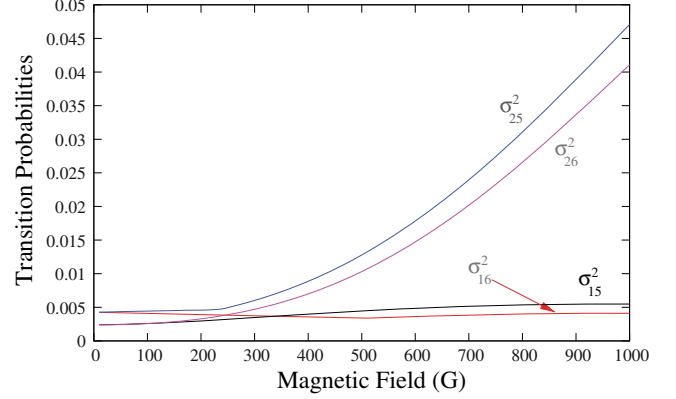


Fig. 7. (Color online) Transition probabilities (σ_{ij}^2) between levels i and j as a function of a magnetic field perpendicular to the crystal Z -axis.

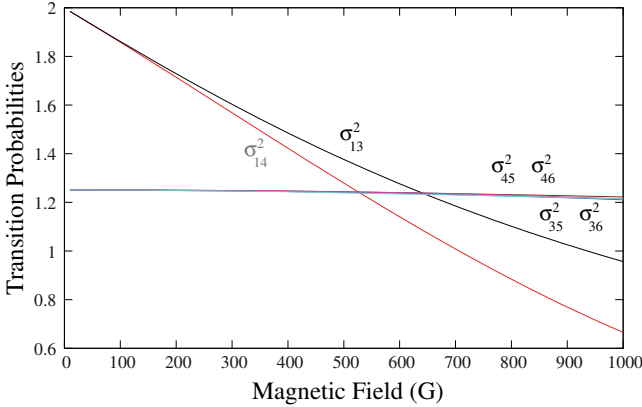


Fig. 6. (Color online) Transition probabilities (σ_{ij}^2) between levels i and j as a function of a magnetic field perpendicular to the crystal Z -axis.

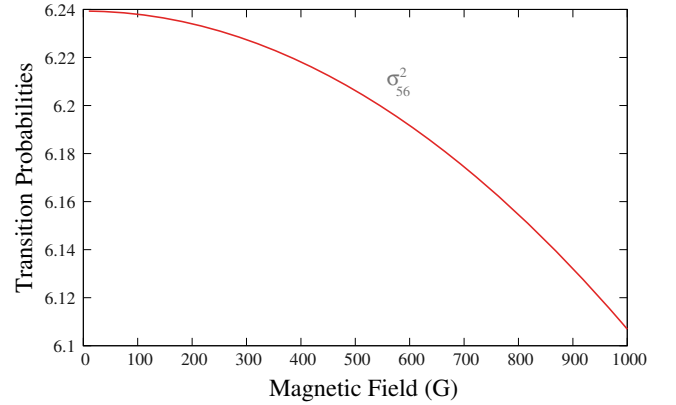


Fig. 8. (Color online) Transition probabilities between levels 5 and 6 as a function of a magnetic field perpendicular to the crystal Z -axis.

a Gaussian normal distribution:

$$g(\nu) = \frac{1}{\sigma\sqrt{2\pi}} \text{Exp} \left[-\frac{1}{2} \left(\frac{\nu - \nu_p}{\sigma} \right)^2 \right] \quad (21)$$

with $\sigma^{-1} = 2\tau_2\sqrt{2\pi}$ [10] and where τ_2 is the spin-spin relaxation time equal to 1 ns [19]. The line shape function for the pump and the maser signal was calculated, but on the next plot we represent only the line shape function for the pump signal (see Fig. 9).

As the levels 5 and 6 are only separated by 450 kHz the two line shape functions are very similar and confirm that states 5 and 6 are mixed together.

5 Evolution of the maser output power and pump power threshold

To determine an order of magnitude of these powers we will consider the parameters at 4.2 K of one of our resonators [18]: the total population is $N = 3.8 \times 10^{20}$ ions/m³, the effective volumes of the WGM are $V_{14} = V_p = 11.7 \times 10^{-6}$ m³. $Q_{0s} = 686 \times 10^6$, $Q_{0p} = 10^8$ and $Z_c = 112 \Omega$.

On the two next plots we have represented the evolution of the pump power threshold and the maser output power as a function of the orientation of the magnetic field and its amplitude.

As we can see in Figure 10 the orientation of the magnetic field has no influence on the maser output power

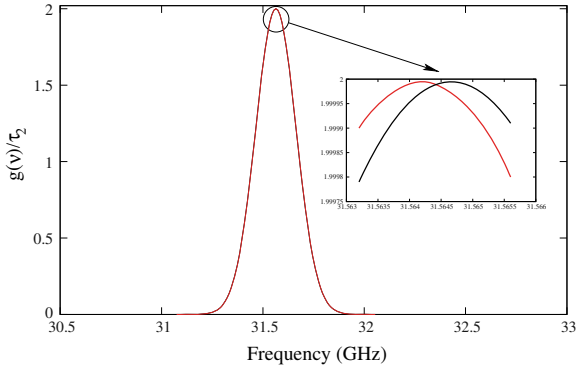


Fig. 9. (Color online) $g(\nu_{15})$ and $g(\nu_{16})$ as a function of ν_p (GHz) for a magnetic field of 50 G perpendicular to the crystal Z-axis.

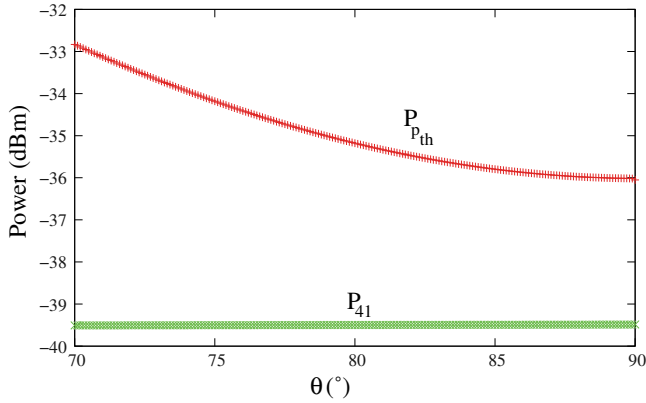


Fig. 10. (Color online) Evolution of the maximum emitted power and pump threshold as a function of the orientation of the magnetic field, for a magnetic field of 50 G.

while for the pump power threshold it is minimum for an angle of 90° . Moreover when the magnetic field increases (Fig. 11) the pump power threshold also increases and the maser output power is still constant over 500 G before decreasing. These two curves confirm our choice to work at a low-level magnetic field (50 G) perpendicular to the crystal Z-axis.

The last plot represents the comparison between the maser output power without and with a magnetic field (50 G, 90°) (see Fig. 12).

The use of magnetic field enables us to increase the maser output power of 6 dB.

6 Conclusion

A complete model of the Whispering Gallery Mode maser under magnetic field was developed. The eigenvectors and the eigenvalues of the Fe^{3+} ion Hamiltonian in the sapphire lattice were calculated in order to determine all the transition probabilities, energy levels, etc.

A general relation between the maser output power and the pump power was also determined. From this calculation we have demonstrated that the use of a magnetic

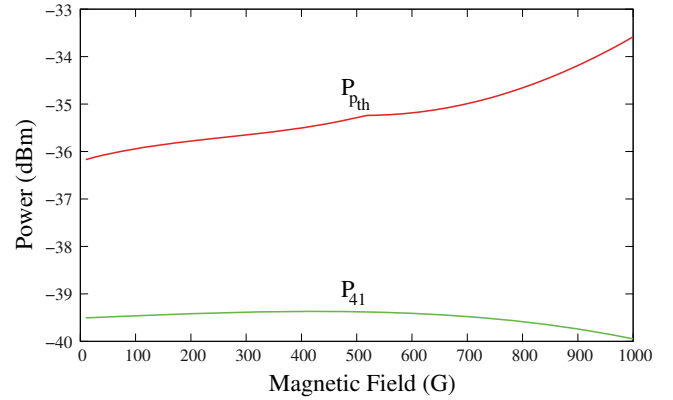


Fig. 11. (Color online) Evolution of the maximum emitted power and pump power threshold as a function of the magnetic field perpendicular to the crystal Z-axis.

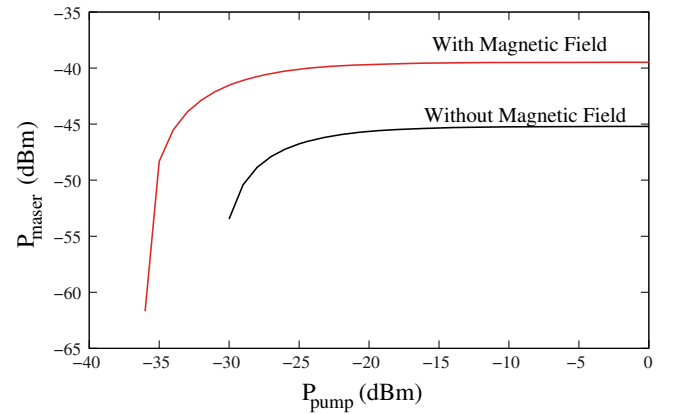


Fig. 12. (Color online) Evolution of the maximum emitted power as a function of the pump power with and without magnetic field. The magnetic field is perpendicular to the crystal Z-axis with a value of 50 G.

field perpendicular to the crystal axis and with an amplitude of 50 G can increase the maser output power by a factor of 6 dB, and also that the pump power threshold can be reduced.

References

1. S. Grop, P.-Y. Bourgeois, N. Basin, Y. Kersalé, E. Rubiola, C. Langham, M. Oxborrow, D. Clapton, S. Walker, J. De Vicente, V. Giordano, *Rev. Sci. Instrum.* **81**, 025102 (2010)
2. J.G. Hartnett, C.R. Locke, E.N. Ivanov, M.E. Tobar, P.L. Stanwix, *Appl. Phys. Lett.* **89**, 203513 (2006)
3. P.-Y. Bourgeois, N. Bazin, Y. Kersalé, V. Giordano, M.E. Tobar, M. Oxborrow, *Appl. Phys. Lett.* **87**, 224104 (2005)
4. P.-Y. Bourgeois, M. Oxborrow, M.E. Tobar, N. Bazin, Y. Kersalé, V. Giordano, *Int. J. Mod. Phys. B* **20**, 1606 (2006)
5. K. Benmessai, P.-Y. Bourgeois, Y. Kersalé, N. Bazin, M.E. Tobar, J.G. Hartnett, M. Oxborrow, V. Giordano, *Electron. Lett.* **43**, 1436 (2007)

6. A.L. Schawlow, C.H. Townes, Phys. Rev. **112**, 1940 (1958)
7. N. Bloembergen, Phys. Rev. **104**, 324 (1956)
8. G.S. Bogle, H.F. Symmons, Proc. Phys. Soc. **73**, 531 (1959)
9. L.S. Kornienko, A.M. Prokhorov, Sov. Phys. JETP **36**, 649 (1959)
10. A.E. Siegman, *Microwave Solid State Masers* (McGraw-Hill, New York, 1964)
11. G.E. Friedman, A.W. Nagy, Proc. IEEE **51**, 361 (1963)
12. D.L. Creedon, K. Benmessai, M.E. Tobar, J.G. Hartnett, P.-Y. Bourgeois, Y. Kersalé, J.-M. Le Floch, V. Giordano, IEEE Trans. Ultrason. Ferroelectr. Freq. Control **57**, 641 (2010)
13. K. Benmessai, D.L. Creedon, M.E. Tobar, P.-Y. Bourgeois, Y. Kersalé, V. Giordano, Phys. Rev. Lett. **100**, 233901 (2008)
14. H.F. Symmons, G.S. Bogle, Proc. Phys. Soc. **79**, 468 (1962)
15. H.H. Wickman, G.K. Wertheim, Phys. Rev. **148**, 211 (1966)
16. L.S. Kornienko, A.M. Prokhorov, Sov. Phys. JETP **40**, 1594 (1961)
17. J.H. Pace, D.F. Sampson, J.S. Thorp, Proc. Phys. Soc. **76**, 697 (1961)
18. K. Benmessai, P.-Y. Bourgeois, M.E. Tobar, N. Bazin, Y. Kersalé, V. Giordano, Meas. Sci. Technol. **21**, 025902 (2010)
19. P.-Y. Bourgeois, K. Benmessai, M. Oxborrow, M.E. Tobar, N. Bazin, J.G. Hartnett, Y. Kersalé, V. Giordano, in *Proc. IEEE IFCS, Genève, CH, 2007*, p. 1031